



OPEN

SUBJECT AREAS:
ORGANIC LEDs
PHOTONIC DEVICESReceived
31 July 2014Accepted
20 November 2014Published
19 December 2014Correspondence and
requests for materials
should be addressed to
C.-I.W. (chihwu@ntu.
edu.tw)

Alternating Current Driven Organic Light Emitting Diodes Using Lithium Fluoride Insulating Layers

Shang-Yi Liu¹, Jung-Hung Chang¹, I.-Wen Wu¹ & Chih-I Wu^{1,2}¹Graduate Institute of Photonics and Optoelectronics, National Taiwan University, Taipei 106, Taiwan, ²Department of Electrical and Engineering, National Taiwan University, Taipei 106, Taiwan.

We demonstrate an alternating current (AC)-driven organic light emitting diodes (OLED) with lithium fluoride (LiF) insulating layers fabricated using simple thermal evaporation. Thermal evaporated LiF provides high stability and excellent capacitance for insulating layers in AC devices. The device requires a relatively low turn-on voltage of 7.1 V with maximum luminance of 87 cd/m² obtained at 10 kHz and 15 Vrms. Ultraviolet photoemission spectroscopy and inverse photoemission spectroscopy are employed simultaneously to examine the electronic band structure of the materials in AC-driven OLED and to elucidate the operating mechanism, optical properties and electrical characteristics. The time-resolved luminance is also used to verify the device performance when driven by AC voltage.

As solid state lighting has attracted a great deal of attention in recent years, light-emitting diodes (LEDs) based on inorganic materials have been investigated and found applications in industry. Although LEDs have reached high efficiency and considerable reliability, they have mostly been designed to be driven by direct current (DC), which differs from household power supplies. As a result, much research has aimed at switching alternating current (AC) voltage input to a DC bias, using devices such as bridge-diode rectifiers and power factor correctors (PFC)^{1,2}. To avoid external electrical circuit modulation, the concept of an AC-driven thin-film electroluminescent (ACTFEL) display was developed³. By sandwiching electroluminescent phosphors between top and bottom insulators, this device features no external carrier injection but is illuminated by field emission and tunneling carriers from interface states. Numerous groups have made significant efforts in inorganic⁴ and organic materials^{5,6} to implement ACTFEL displays using various phosphors embedded in their devices. In particular, it would be great to drive organic LEDs (OLEDs), which possess the potential to reach nearly 100% internal quantum efficiency^{7,8} and becomes the candidate as the next generation lighting sources^{9,10}, with AC current and voltages.

However, the insulators in AC-driven devices procure limited free carriers for recombination, resulting in extremely high operating voltages. This has motivated several groups to increase interior carriers by inserting conducting-doping layers¹¹ or charge generation centers within the devices^{12,13}. Leo's group simply replaced the electroluminescent phosphor layers in ACTFEL devices with specific functional layers and selected hafnium dioxide as a high-k insulator^{14–16}, which greatly reduced operating voltage and raised output brightness of the AC electroluminescence (ACEL) devices. Further works also emphasized structural adjustment to achieve maximum optical performance¹⁵, optimized operating frequency¹⁴, and white light emission¹⁷. Although ACEL devices have attained improved characteristics, the use of the insulating layers, such as ALD hafnium dioxide and silicon dioxide, is rarely used in OLED processes and would cause some manufacture difficulties. In addition, the operating mechanism of ACEL devices requires systematic investigation to facilitate further improvements.

In this study, we demonstrate an AC-driven OLED, with lithium fluoride (LiF) as its insulating layer using a simple thermal evaporation process. The thermally deposited LiF exhibits excellent insulation and capacitance for its wide band gap¹⁸ and relatively high k ¹⁹ compared to SiO₂, and is more easily processed along with organic materials²⁰. Ultraviolet photoelectron spectroscopy (UPS) and inverse photoemission spectroscopy (IPES) are employed to examine the electronic band structure of AC-driven OLEDs to explore the operation mechanisms.

Results

The bottom-emitting AC-driven OLED structure involved in this work is illustrated in Fig. 1. Molybdenum trioxide acts as a p-type dopant for N,N'-Bis(naphthalen-1-yl)-N,N'-bis(phenyl)benzidine (NPB) due to its deep

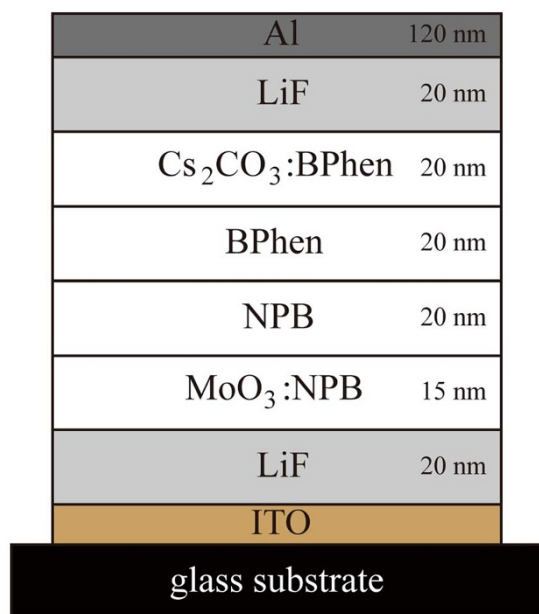


Figure 1 | AC-driven OLED device structure.

conduction band and chemical reaction with NPB, forming a p-type layer for hole donating. An n-type layer including cesium carbonate was reported for its effective charge transfer to 4,7-Diphenyl-1,10-phenanthroline (BPhen), leading to massive increases in electron

concentration^{21,22}. A bilayer emission unit consisting of NPB and BPhen for hole and electron transport, respectively, was sandwiched between the p-type and n-type layers. The LiF insulating layers were inserted between the organic layers and electrodes to create a device illuminated by internal carriers.

To investigate the mechanism of free carrier generation and transport in AC-driven OLEDs, UPS and IPES measurements were carried out simultaneously with four functional layers deposited sequentially. First of all, a 5 nm p-type NPB layer, MoO₃:NPB, was deposited on a clean Au substrate. As shown in Fig. 2a, the highest occupied molecular orbit (HOMO) edge of the MoO₃:NPB layer is 0.35 eV below the Fermi level (E_F), which verifies the p-type doping properties of MoO₃²³. Then, 20-nm pristine NPB was incrementally deposited. With increasing pristine NPB thickness, the photoemission onset and the occupied valence state features of NPB gradually shift to higher binding energy. The results of photoemission measurements of 20-nm pristine NPB on the 5-nm MoO₃:NPB layer are shown in Fig. 2b; the HOMO edge of 20-nm pristine NPB is 0.85 eV below the E_F . Compared with pristine NPB on a clean Au substrate, this pristine NPB still shows p-type properties due to the p-type NPB layer beneath, which is doped with MoO₃. To study the NPB/BPhen interface, a 20-nm BPhen layer was deposited on an Au/MoO₃:NPB (5 nm)/NPB (20 nm) substrate and the results of UPS and IPES are shown in Fig. 2c. From the photoemission results, the lowest unoccupied molecular orbit (LUMO) edge of 20 nm BPhen on the NPB layer is 1.65 eV above the E_F and the HOMO edge is 2.55 eV below the E_F . Finally, BPhen doped with Cs₂CO₃ as an n-type layer was deposited on the pristine BPhen layer. Compared with pristine BPhen, the photoemission onset shifts to higher binding energy

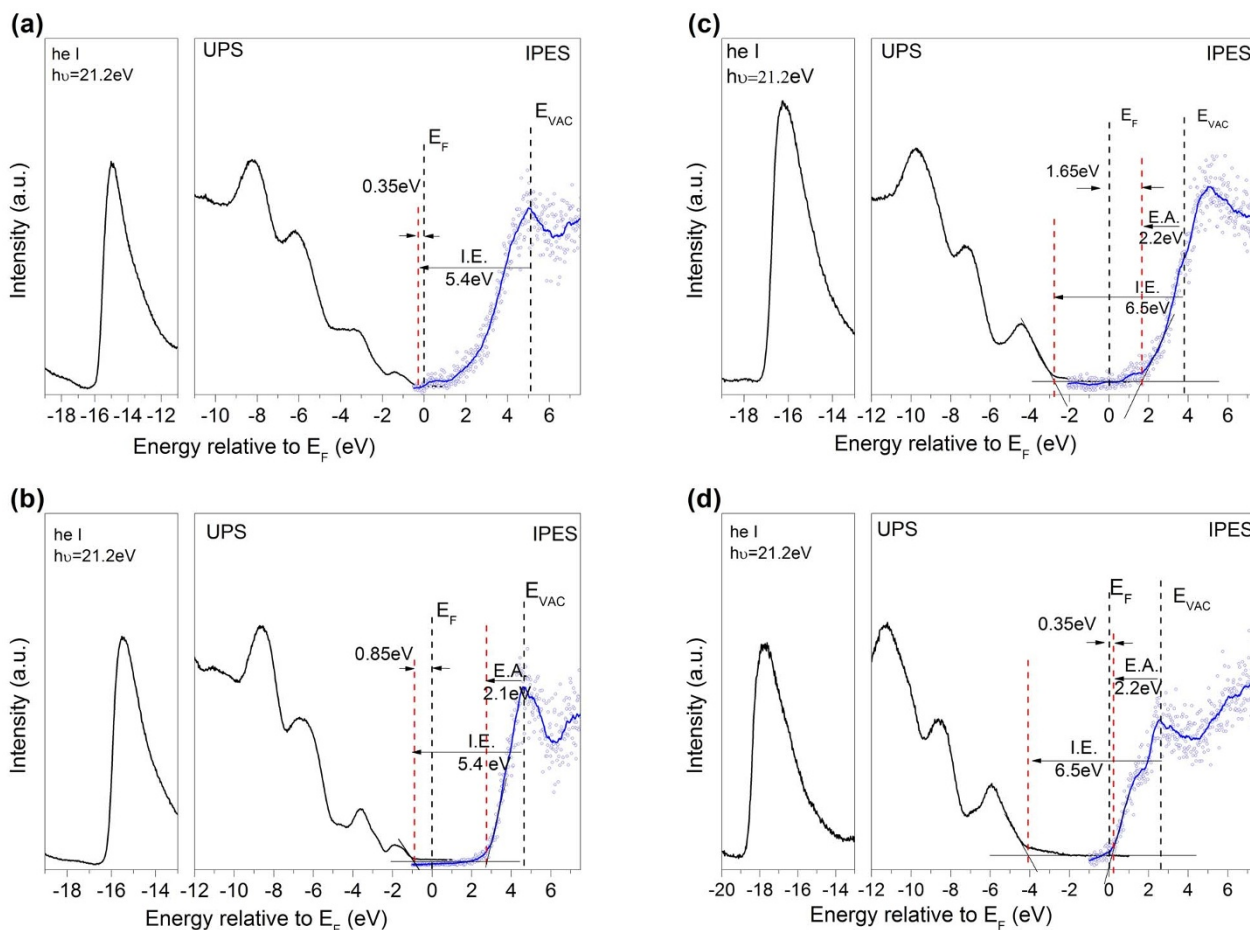


Figure 2 | UPS (black) and IPES (blue) results for structures of (a) MoO₃:NPB on Au (b) NPB on Au/MoO₃:NPB (c) BPhen on Au/MoO₃:NPB/NPB (d) Cs₂CO₃:BPhen on Au/MoO₃:NPB/NPB/BPhen.

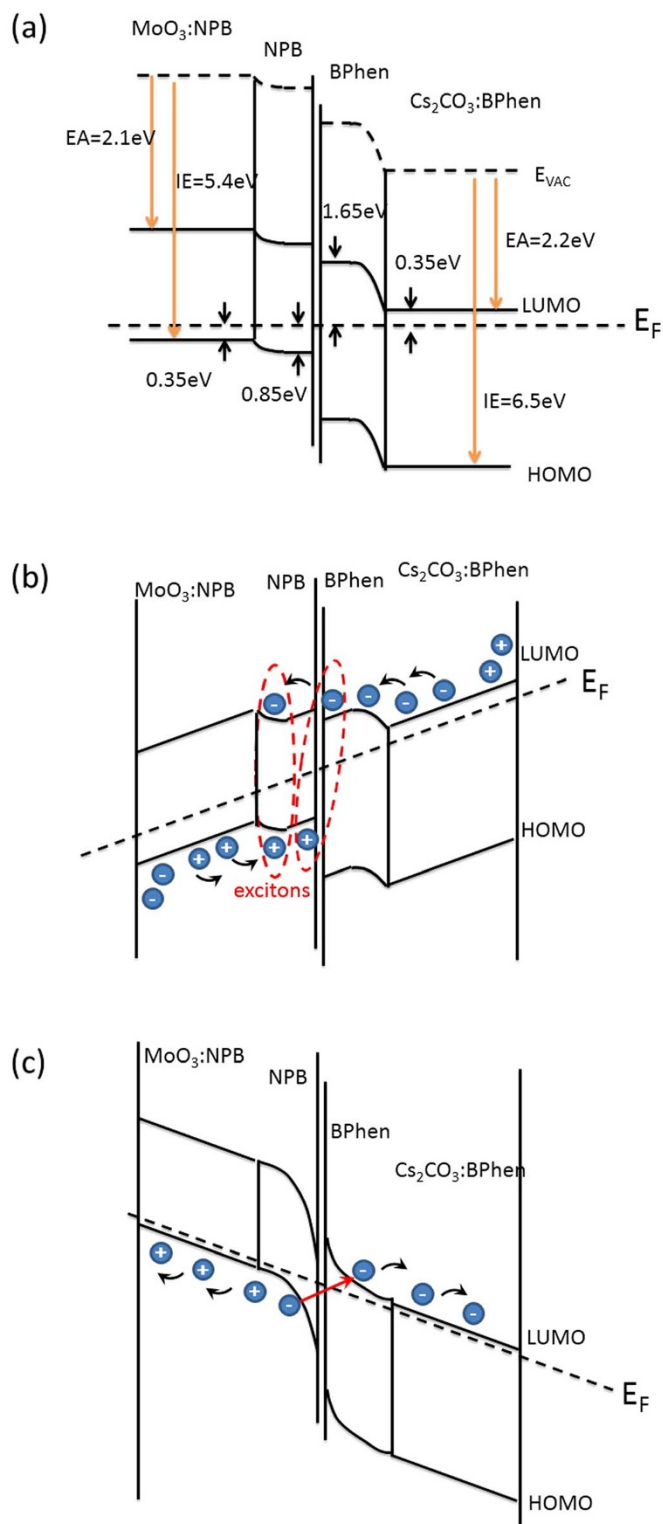


Figure 3 | (a): Electronic band structure corresponding to UPS and IPES results. (b): Energy band diagram of AC-driven OLED in forward cycles of AC voltage. (c): Energy band diagram of AC-driven OLED in reverse cycles of AC voltage.

and the LUMO edge becomes closer to the E_F as the $\text{Cs}_2\text{CO}_3\text{:BPhen}$ layer increases. Fig. 2d shows that the LUMO edge of the 20-nm $\text{Cs}_2\text{CO}_3\text{:BPhen}$ layer is 0.35 eV above the E_F , demonstrating that the film is indeed highly n-doped. A summary of the energetic alignments of the AC-driven OLED structure is given in Fig. 3.

The correlation between AC voltage and luminance is shown in Fig. 4, with a log scale in the inset. Turn-on voltages (defined as voltage at which the luminance reaches a level of 1 Cd/m^2) at different frequencies are observed to be similar at around 7.1 V, which is greatly reduced compared to previous research¹⁵. Above the turn-on voltage, applied electric fields in the device increase proportionally so that luminance rises linearly with voltage. In addition, higher luminance is detected at higher frequency, which can be attributed to a decrease in capacitive reactance with increasing frequency. With DC bias, only background signal in the black box is detected, regardless the DC voltage. These results imply that these devices only illuminate when they are driven by AC.

Discussion

The summary of the energetic alignments of the AC-driven OLED structure given in Fig. 3(a) can be used to explain the behavior of charge generation and transport in the AC-driven OLED, and the schematics of energy band diagram in forward and reverse cycles are shown in Fig. 3(b) and 3(c), respectively. As NPB doped with MoO_3 , this electric doping effect provides holes at the HOMO of $\text{MoO}_3\text{:NPB}$ layer without external injection. In forward cycles, the forward electric field moves the holes to the HOMO states of undoped NPB layers, and the electrons in the HOMO of NPB layers are reversely drifted to the HOMO of $\text{MoO}_3\text{:NPB}$ layer in the same time. These electrons are likely to accumulate near the interface of insulating layer (LiF) and $\text{MoO}_3\text{:NPB}$ layer. Similarly, $\text{Cs}_2\text{CO}_3\text{:BPhen}$ layer is full of mobile electrons at its LUMO via electric doping. In forward cycles, the free electrons in the LUMO of $\text{Cs}_2\text{CO}_3\text{:BPhen}$ layer drift to the LUMO of BPhen and hence NPB, and the equivalent amount of positive charges drift to $\text{Cs}_2\text{CO}_3\text{:BPhen}$ layer and accumulate near the interface of insulating layer. The excitons are generated in NPB and at the interface of NPB and BPhen, and then recombine. As the applied AC voltage switches to reverse cycles, the applied reverse electric field yields a tilted Fermi level illustrated in Fig. 3(c). The built-in energy band bending observed at the p-type NPB/undoped NPB and undoped BPhen/n-type BPhen interface becomes more pronounced, and the width of tunneling barrier is reduced as well²⁴. After the excitons recombine in forward cycles, the free electrons in the LUMO of NPB and BPhen relax to the HOMO of NPB. In reverse cycles, these de-excited electrons are moved by the reverse electric field and encounter the energy barrier at NPB/BPhen interface and tunnel to the LUMO of BPhen. After the electrons tunnel to the LUMO of BPhen, equivalent amount of electron vacancies (holes), are generated in the HOMO of NPB. These free electrons and holes are drifted by the reverse field and transit to the LUMO of n-type BPhen and the HOMO of p-type NPB, respectively. As the holes and free electrons transit to the p and n-type layer, the accumulated charges in forward cycles are exchanged for these free carriers. The whole device returns to ground and neutralized states. This whole charge regeneration is then completed.

We fabricated single-layer devices with a structure of ITO/LiF/Al to measure the properties of the LiF films. To investigate the electrical properties of these single-layer devices, various thicknesses of LiF, including 10, 15, and 20 nm, were deposited at multiple rates ranging from 0.01 to 0.03 nm/s. Fig. 5a shows the current density of these devices driven at a DC voltage bias of 20 V, plotted with respect to corresponding deposition rates. For LiF deposited at the same rate, relatively large leakage current are found for the single-layer device with 10 nm and 15 nm thick LiF. When the thickness of LiF reached 20 nm, a severe current drop can be observed, which imply that tunneling current dominates until the thickness of LiF approaches 20 nm. In addition, a lower leakage current is measured in the single-layer device fabricated with LiF deposited at a lower rate. These results are consistent with the capacitances of 20 nm thick LiF, found to be 7.01 nF, 5.44 nF, and 4.71 nF in single-layer devices with deposition rates of 0.01 nm/s, 0.02 nm/s, 0.03 nm/s, respectively,

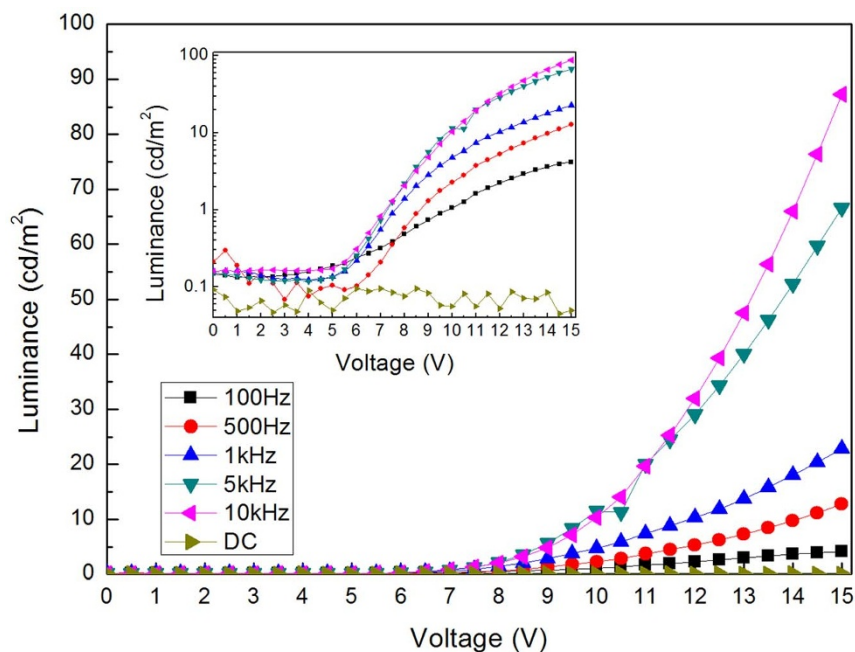


Figure 4 | AC and DC current density-voltage (J - V) characteristics of AC-driven OLED. Luminance driven by AC voltage at different frequencies are plotted in linear scale and DC voltage input with log scale in the inset.

indicating that a denser formation of LiF is achieved by a smaller deposition rate.

Further insight into charge recombination within the AC-driven OLED is achieved by comparing two devices with and without insulating layers, the latter being a typical DC-driven OLED. The DC current densities of AC and DC-driven OLEDs are shown in Fig. 5b. A diode-like current density-voltage curve is observed in the DC-driven OLED in Fig. 5b with a turn-on voltage of 2 V, showing an effective charge recombination and injection provided by p-type and n-type layers. In contrast, the AC-driven OLED exhibits an extremely small current density in DC bias due to the excellent functioning of the LiF insulating layer, which indicates that the AC-driven OLED illuminates by internal charge recombination instead of external injection current. Fig. 5c shows the electroluminescence (EL) spectra of AC and DC-driven OLEDs. The EL spectrum of the AC-driven OLED features two remarkable peaks at 450 and 496 nm with nearly equivalent intensity. Similarly, the EL spectrum of the DC-driven OLED contains the two peaks at the same wavelengths, while the peak at 450 nm is smaller in intensity as compared to that at 496 nm. The EL peak detected at 450 nm is identical to the photoluminescence (PL) spectrum of NPB in peak wavelength position²⁵, indicating that portions of the excitons are formed and recombined in NPB. In Fig. 3, holes from the p-type layer in the forward

cycles are likely to accumulate at the interface of NPB and BPhen due to the large energy difference in the HOMOs of NPB and BPhen. An interfacial exciplex created by an electron in BPhen and a hole in NPB leads to an exciplex emission observed in longer wavelengths. The exciplex recombines and generates a photon originating from the 2.5 eV energy difference in the LUMO of BPhen and the HOMO of NPB, which is consistent to the EL peak located at the wavelength of 496 nm. To investigate the intensity ratio of the two peaks, the EL spectra of the DC-driven OLED at multiple DC voltages ranging from 3.5 to 5.5 V are displayed in Fig. 6. Fig. 6a shows a majority of the emission is contributed by the interfacial exciplexes and a relatively small portion of the recombination occurs in NPB. As we increase DC voltage, the proportion of NPB fluorescence gradually increases and reaches comparable intensity to interfacial exciplex emission. The results suggest that lower applied voltage provides insufficient intensity of electric field within the device such that electrons in BPhen are partially blocked by the energy barrier between the LUMOs of NPB and BPhen. At higher applied voltages, more electrons in BPhen overcome the energy barrier, generating more excitons formed in NPB for NPB fluorescence. The voltage-dependent EL spectrum displays more balanced emission from fluorescence and exciplexes at high voltages, which is consistent with the previous report²⁶. In Fig. 5c, when the AC-driven OLED is operated

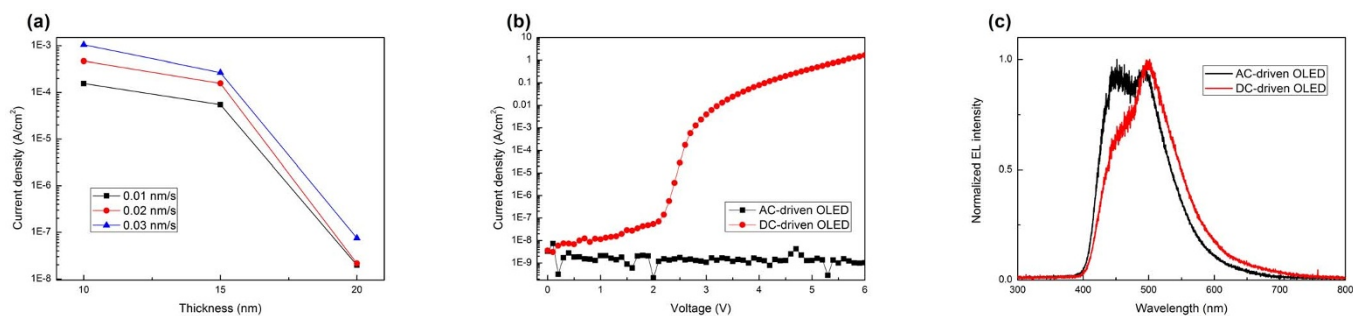


Figure 5 | (a): DC current density of single-layer LiF (device structure: ITO/LiF/Al) at different deposition rates and thicknesses. (b): DC J - V characteristics of AC-driven OLED (with insulating layer) and DC-driven OLED (without insulating layer). (c): electroluminescence (EL) spectra of AC and DC-driven OLEDs. NPB fluorescence and interfacial exciplex emission are observed at 450 and 496 nm respectively.

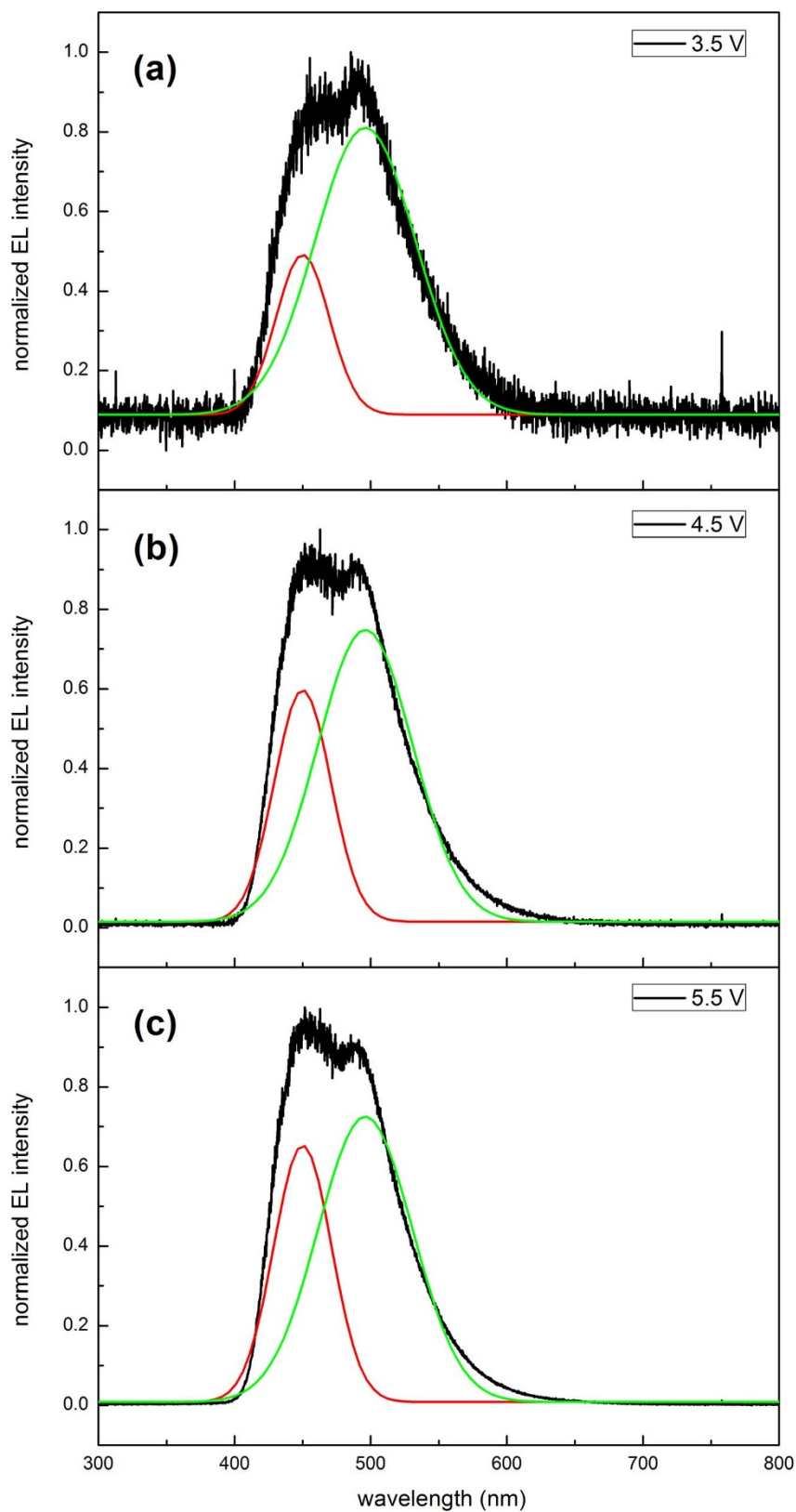


Figure 6 | EL spectra of DC-driven OLED at multiple DC input voltages of (a) 3.5 V (b) 4.5 V (c) 5.5 V with Gaussian peak fitting of NPB fluorescence (peaked at 450 nm) and interfacial exciplex (peaked at 496 nm).

at relatively high voltages, a larger proportion of NPB fluorescence is observed in the EL spectrum compared with the DC-driven OLED. Because the photodiode accumulates all luminance in the entire cycle of AC voltage, the EL spectrum collects responses from all voltages

within the cycle and exhibits an average spectrum of the emission, and hence fluorescence from NPB and interfacial exciplexes equally contribute to the EL spectrum of the AC-driven OLED, resulting in the same height of the two peaks.

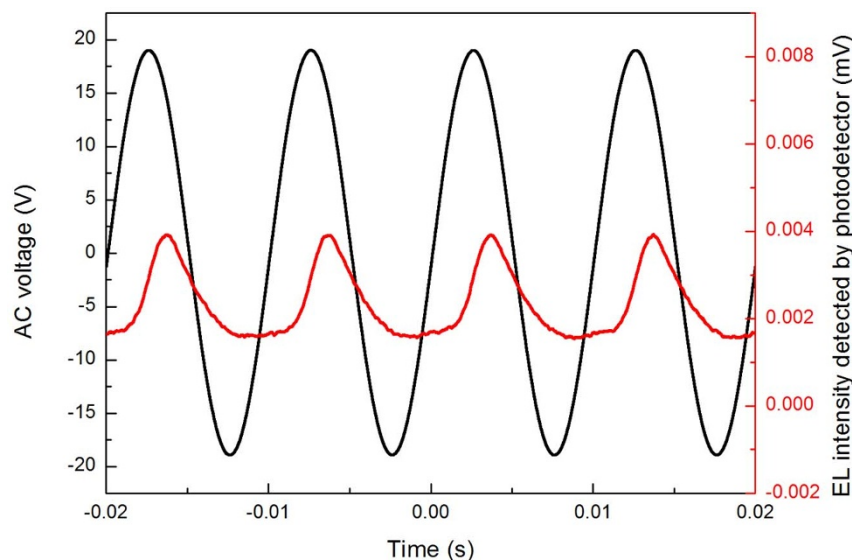


Figure 7 | Time-resolved luminance of AC-driven OLED with AC voltage at 100 Hz. The device is illuminated only in forward half-cycles.

Fig. 7 shows the time-resolved luminance plotted in conjunction with its AC driving voltage of 18 Vrms at 100 Hz. A notable increase of luminance is observed in the forward half-cycles of the input AC voltage, while the delayed response indicates illumination above the turn-on voltage. In reverse half-cycles, no luminous response is detected. From the band structure of the AC-driven OLED illustrated in Fig. 2, photon recombination would occur only in forward half-cycles and no luminance would be output during charge generation in reverse half-cycles, which fully agrees with the result shown in Fig. 7.

In conclusion, we have demonstrated an AC-driven OLED with LiF insulating layers, fabricated by simple thermal evaporation with excellent insulation and capacitance behaviors. UPS and IPES particularly illustrate the electronic band structure of the AC-driven OLED, explicitly describing its electrical and optical properties. The device features frequency-dependent luminance, balanced emission of NPB fluorescence and exciplexes, and highly reduced turn-on voltage, with a maximum AC luminance of 87 cd/m² at 15 V and 10 kHz. Both DC electrical characteristics and time-resolved luminance clearly reveal that the device operates effectively with only AC voltage input.

Methods

A commercial 120 nm thick ITO-coated glass substrate was cleaned in acetone, methanol, and DI water for 10 minutes sequentially in an ultrasonic bath. Before device fabrication, the as-prepared substrate was treated by UV ozone for 10 minutes and then immediately transferred into a thermal deposition chamber. Sublimated sources were evaporated in the chamber with a base pressure of 10⁻⁶ torr and equipped with an in-situ mask changing system.

Photoemission experiments were carried out by UPS and IPES simultaneously in an ultra-high vacuum chamber with a base pressure of 1 × 10⁻¹⁰ torr. The photon energy in UPS experiments is 21.2 eV of He I excitation with an experimental resolution of 0.15 eV, and the kinetic energy of photoelectrons was measured by a cylindrical mirror analyzer. IPES was carried out in the isochromat mode with a resolution of around 0.45 eV^{27,28}. The Fermi level reference in UPS and IPES was established by a clean Au surface. All the organic and inorganic films were prepared in a deposition chamber and transferred in situ to the analysis chamber without breaking the vacuum, to study the electronic structure by UPS and IPES.

The AC and DC analysis was measured by an Agilent E4980A LCR meter and a Keithley 2400 source meter, respectively. Luminance from all devices was detected by a commercial photodiode in a black box, and the AC voltage signal was collected by an oscilloscope for time-resolved luminance. The EL spectra at various wavelengths are collected by a commercial photo-coupler from Ocean Optics.

1. Li, Y. C. & Chen, C. L. A Novel Single-Stage High-Power-Factor AC-to-DC LED Driving Circuit With Leakage Inductance Energy Recycling. *IEEE T. Ind. Electron.* **59**, 793–802 (2012).

2. Moschopoulos, G. & Jain, P. Single-phase single-stage power-factor-corrected converter topologies. *IEEE T. Ind. Electron.* **52**, 23–35 (2005).
3. Rack, P. D. & Holloway, P. H. The structure, device physics, and material properties of thin film electroluminescent displays. *Mat. Sci. Eng. R.* **21**, 171–219 (1998).
4. Bredol, M. & Dieckhoff, H. S. Materials for Powder-Based AC-Electroluminescence. *Materials.* **3**, 1353–1374 (2010).
5. Xu, X. L. *et al.* Blue electroluminescence from tris-(8-hydroxyquinoline) aluminum thin film. *Chem. Phys. Lett.* **325**, 420–424 (2000).
6. Yang, S. Y., Qian, L., Teng, F., Xu, Z. & Xu, X. R. Alternating-current electroluminescence from an organic heterojunction sandwiched between two amorphous SiO₂ layers. *J. Appl. Phys.* **97**, 126101 (2005).
7. Adachi, C., Baldo, M. A., Thompson, M. E. & Forrest, S. R. Nearly 100% internal phosphorescence efficiency in an organic light-emitting device. *J. Appl. Phys.* **90**, 5048 (2001).
8. Kawamura, Y. *et al.* 100% phosphorescence quantum efficiency of Ir(III) complexes in organic semiconductor films. *Appl. Phys. Lett.* **86**, 071104 (2005).
9. Kido, J., Kimura, M. & Nagai, K. Multilayer White Light-Emitting Organic Electroluminescent Device. *Science.* **267**, 1332–1334 (1995).
10. Liao, L. S., Klubek, K. P. & Tang, C. W. High-efficiency tandem organic light-emitting diodes. *Appl. Phys. Lett.* **84**, 167 (2004).
11. Perumal, A. *et al.* Novel Approach for Alternating Current (AC)-Driven Organic Light-Emitting Devices. *Adv. Funct. Mater.* **22**, 210–217 (2012).
12. Lee, S.-B., Fujita, K. & Tsutsui, T. Emission Mechanism of Double-Insulating Organic Electroluminescence Device Driven at AC Voltage. *Jpn. J. Appl. Phys.* **44**, 6607–6611 (2005).
13. Tsutsui, T., Lee, S.-B. & Fujita, K. Charge recombination electroluminescence in organic thin-film devices without charge injection from external electrodes. *Appl. Phys. Lett.* **85**, 2382 (2004).
14. Fröbel, M. *et al.* Enhancing the efficiency of alternating current driven organic light-emitting devices by optimizing the operation frequency. *Org. Electron.* **14**, 809–813 (2013).
15. Perumal, A., Lüssem, B. & Leo, K. Ultra-bright alternating current organic electroluminescence. *Org. Electron.* **13**, 1589–1593 (2012).
16. Perumal, A., Lüssem, B. r. & Leo, K. High brightness alternating current electroluminescence with organic light emitting material. *Appl. Phys. Lett.* **100**, 103307 (2012).
17. Fröbel, M. *et al.* White light emission from alternating current organic light-emitting devices using high frequency color-mixing. *Phys. Status Solidi A.* **210**, 2439–2444 (2013).
18. Chaney, R., Lafon, E. & Lin, C. Energy Band Structure of Lithium Fluoride Crystals by the Method of Tight Binding. *Phys. Rev. B.* **4**, 2734–2741 (1971).
19. Andeen, C., Fontanella, J. & Schuele, D. Low-Frequency Dielectric Constant of LiF, NaF, NaCl, NaBr, KCl, and KBr by the Method of Substitution. *Phys. Rev. B.* **2**, 5068–5073 (1970).
20. Hung, L. S., Tang, C. W. & Mason, M. G. Enhanced electron injection in organic electroluminescence devices using an Al/LiF electrode. *Appl. Phys. Lett.* **70**, 152–154 (1997).
21. Chen, M. H. & Wu, C. I. The roles of thermally evaporated cesium carbonate to enhance the electron injection in organic light emitting devices. *J. Appl. Phys.* **104**, 113713 (2008).
22. Wu, C. I. *et al.* Electronic structures and electron-injection mechanisms of cesium-carbonate-incorporated cathode structures for organic light-emitting devices. *Appl. Phys. Lett.* **88**, 152104 (2006).



23. Wu, C. I. *et al.* Electronic and chemical properties of molybdenum oxide doped hole injection layers in organic light emitting diodes. *J. Appl. Phys.* **105**, 033717 (2009).
24. Kleemann, H. *et al.* Organic Zener Diodes: Tunneling across the Gap in Organic Semiconductor Materials. *Nano Lett.* **10**, 4929–4934 (2010).
25. Song, Q. L. *et al.* Exciton dissociation in organic light emitting diodes at the donor-acceptor interface. *Phys. Rev. Lett.* **98**, 176403 (2007).
26. Yu, J., Lou, S., Wen, W., Jiang, Y. & Zhang, Q. Color-tunable organic light emitting diodes based on exciplex emission. *Proc. SPIE.* **7282**, 728234 (2009).
27. Wu, C. I., Hirose, Y., Sirringhaus, H. & Kahn, A. Electron-hole interaction energy in the organic molecular semiconductor PTCD A. *Chem. Phys. Lett.* **272**, 43–47 (1997).
28. Wu, C. I. & Kahn, A. Electronic states at aluminum nitride (0001)-1x1 surfaces. *Appl. Phys. Lett.* **74**, 546–548 (1999).

Acknowledgments

This work is supported by National Science Council of the Republic of China (NSC 101-2628-M-002-004-MY3 and NSC 102-2622-E-002-014) and the Center for Emerging Materials and Advanced Devices, National Taiwan University.

Author contributions

S.Y.L. designed and performed the experiments with data analysis; I.W.W. carried out the AC analysis. J.H.C. helped with the device fabrication. C.I.W. provided the advice on and coordinated the experiments. S.Y.L. and C.I.W. wrote the manuscript and all authors contributed equally towards improving it.

Additional information

Competing financial interests: The authors declare no competing financial interests.

How to cite this article: Liu, S.-Y., Chang, J.-H., Wu, I.-W. & Wu, C.-I. Alternating Current Driven Organic Light Emitting Diodes Using Lithium Fluoride Insulating Layers. *Sci. Rep.* **4**, 7559; DOI:10.1038/srep07559 (2014).



This work is licensed under a Creative Commons Attribution-NonCommercial-NoDerivs 4.0 International License. The images or other third party material in this article are included in the article's Creative Commons license, unless indicated otherwise in the credit line; if the material is not included under the Creative Commons license, users will need to obtain permission from the license holder in order to reproduce the material. To view a copy of this license, visit <http://creativecommons.org/licenses/by-nc-nd/4.0/>